Smart Materials and Structures

OPEN ACCESS

RECEIVED
6 January 2026

REVISED
19 March 2026

ACCEPTED FOR PUBLICATION
31 March 2026

PUBLISHED
9 April 2026

PAPER

Tunable shock and vibration damping in metal laser powder bed fusion components via controlled post-print compaction of particle damper cavities

Joud N Satme[1,5], Yanzhou Fu[1,2,5], Samuel Roberts[1], Austin R J Downey[1,3,*], Tianyu Zhang[1], Lang Yuan[1] and Daniel Kiracofe[4]

[1] Department of Mechanical Engineering, University of South Carolina, Columbia, SC 29208, United States of America
[2] Department of Ocean and Mechanical Engineering, Florida Atlantic University, Boca Raton, FL 33431, United States of America
[3] Department of Civil and Environmental Engineering, University of South Carolina, Columbia, SC 29208, United States of America
[4] Beehive Industries, Cincinnati, OH 45140, United States of America
[5] These authors contributed equally to this work.
[*] Author to whom any correspondence should be addressed.

E-mail: austindowney@sc.edu

Keywords: laser powder bed fusion, particle damper, density and volume compression, structural dynamics, vibration change

Abstract

Components manufactured by Laser Powder Bed Fusion (LPBF) can incorporate particle dampers (PDS) by retaining unfused powder within internal pockets, providing inherent vibration suppression without added mass or separate damping components. This study investigates the damping performance of such LPBF-integrated PDs through two complementary approaches: (1) quantifying the effect of post-printing volume compression on energy absorption by mechanically indenting the damper pocket, and (2) evaluating how variations in particle packing density influence the dynamic response under both sinusoidal and transient impulse excitation. Experimental results from shaker and shock testing demonstrate that increased packing density, whether by compression or tighter confinement, reduces damping effectiveness. In shock tests, the PD reduced the quality factor (Q) from 174.8 for the solid beam to 116.7 for the unindented PD, corresponding to an approximate 33% reduction in Q. Indentation of the pocket caused the first-mode modal frequency to shift upward from 416.0 Hz at 0 μm (3.0% below the solid beam) to 428.7 Hz at 111 μm indentation, effectively converging with the solid beam's frequency. A transfer function model is developed to characterize system dynamics and predict modal behavior. Finite element simulations further confirm that the observed vibration suppression stems from the PD itself rather than changes to the pocket geometry. These findings highlight the potential of LPBF-integrated PDs for tailored vibration control in complex structures, enabling multifunctional design in advanced engineering applications.

Abbreviations

The following abbreviations are used in this manuscript:

LPBF	Laser Powder Bed Fusion
Q factor	Quality factor
PD	Particle damper
DEM	Discrete element method
MTS	Material testing systems
IEPE	Integrated electronics piezo-electric
FEM	Finite element method
DEM	discrete element modeling

1. Introduction

Vibration control is critical to the safety, reliability, and longevity of dynamic systems [1]. In applications ranging from aerospace structures to industrial machinery, uncontrolled vibrations can lead to accelerated wear, fatigue failure, and performance degradation [2]. Damping strategies mitigate these effects by converting vibrational kinetic energy into heat or other forms of energy, thereby reducing amplitude and duration [3].

Passive damping techniques are among the most widely used due to their simplicity, robustness, and long-term reliability. They are easy to implement and require minimal maintenance, making them ideal for critical applications where active systems may be impractical. Passive dampers can also be strategically placed within a structure, especially at the antinodes of dominant mode shapes, to reduce localized resonances and improve overall system stability [4]. However, their fixed damping characteristics limit adaptability to changing vibration conditions, and they often require additional mass, space, and multiple components, which can increase complexity and risk of failure. In contrast, active and semi-active damping systems use feedback control to adapt to varying vibration environments in real time [5]. While they offer tunable performance, these systems require sensors, actuators, and power sources, introducing complexity, weight, and maintenance demands. These trade-offs highlight the need for advanced passive damping solutions that offer enhanced performance while maintaining simplicity and reliability.

To address these challenges, emerging additive manufacturing technologies, particularly LPBF, enable the integration of damping functionality directly into structural components [6]. LPBF employs a high-energy laser to selectively melt and fuse metal powders layer-by-layer, allowing for the fabrication of complex geometries with tailored mechanical properties [7]. A novel application of this technique involves intentionally retaining unfused powder inside internal cavities, forming integrated PDs that provide lightweight, space-efficient vibration suppression without requiring additional assemblies or external dampers [8].

The damping mechanism of LPBF-based PDs relies on a combination of inelastic collisions and friction between loose powder particles and cavity walls, which effectively dissipates vibrational energy, especially under high-frequency or transient loading [9]. These attributes make LPBF-integrated PDs especially attractive for aerospace applications, where low mass and high structural integrity are critical.

Despite their promise, several fundamental questions remain. The effects of particle packing density, post-printing changes in pocket volume, and how these factors influence damping behavior across different excitation conditions are not fully understood. Additionally, it is important to distinguish whether vibration suppression arises from particle interactions or merely from geometric modifications to the pocket.

To address these gaps, this study investigates the damping behavior of LPBF-integrated PDs under both shock and continuous sinusoidal excitation and validates the findings through finite element simulations. We examine how mechanical indentation of the damper pocket affects packing density and dynamic response, and develop a transfer function model to characterize system behavior. Finally, FEM simulations confirm that the damping effects stem from particle dynamics rather than pocket geometry alone. This work demonstrates through combined experimental testing and numerical modeling that post-printing indentation can be used to tune damping performance: specifically, compressing the particle pocket reduces Q factor by up to 33% (from 174.8 to 116.7) and shifts the first-mode modal frequency upward toward that of the solid beam. These results establish a practical method for post-tuning vibration characteristics in LPBF components, enabling multifunctional structural designs with embedded damping control. The main contributions of this work are threefold. First, we introduce a systematic experimental framework to quantify how controlled post-printing volume compression influences the damping performance of LPBF-integrated PDs, a novel aspect that has not been previously characterized. Second, we establish the relationship between particle packing density and vibration suppression through combined shock and continuous excitation tests, demonstrating that increased confinement reduces energy dissipation efficiency. Third, we develop and validate a transfer function model and finite element simulations that distinguish the effects of particle interactions from geometric stiffness changes, confirming that damping arises primarily from internal particle dynamics. Collectively, these contributions advance the understanding of tunable, embedded damping mechanisms in LPBF components and present a practical pathway for post-manufacture tuning of vibration behavior in multifunctional structural systems.

2. Literature review

This section provides a comprehensive overview of previous work on LPBF-integrated PDs, focusing on experimental investigations, design optimization, and analytical modeling approaches that have shaped current understanding of their vibration suppression capabilities. It first reviews studies that experimentally characterized damping behavior in LPBF-fabricated structures, followed by research exploring how geometric design and material parameters influence performance. The section then discusses the analytical and computational models developed to describe particle-structure interactions and concludes by identifying key knowledge gaps, particularly regarding the roles of particle packing density and post-printing volume compression, that motivate the present study.

2.1. Experimental investigations of LPBF-integrated PDs

PDs have been extensively studied for their ability to suppress structural vibrations through passive energy dissipation by particle-wall and particle-particle interactions. Owing to their simplicity and sensitivity, cantilever beam configurations are commonly used to characterize damping performance. Ehlers *et al* [10] demonstrated up to 20-fold damping enhancement in LPBF-fabricated AlSi10Mg beams with internal powder cavities ranging from 2 to 5 mm in width. Their study systematically linked the first through seventh bending modes (600–18 000 Hz) to cavity geometry, showing that cavities sized to maintain a packing fraction between 50%–70% provided the most effective energy dissipation. Guo *et al* [11] combined DEM simulations and base-excitation experiments to validate damping mechanisms in LPBF 316 L cantilever beams. They fabricated multi-unit PDs with unit cells of 5–10 mm and found that increasing the number of unit cells proportionally enhanced the specific damping capacity, particularly near the first two resonance peaks below 100 Hz. Schmitz *et al* [12] observed that increasing the powder core width from 2 to 8 mm increased damping by factors of 2.9 to 225, but also altered mode shapes due to stiffness reduction. Their LPBF stainless-steel walls confirmed that excessive cavity dimensions (large than 8 mm) induced modal distortion, highlighting a trade-off between damping and structural integrity. Scott-Emuakpor *et al* [13, 14] established that 1%–4% retained unfused powder volume within LPBF components can yield 88%–95% vibration suppression compared to fully fused structures. Their long-duration endurance testing showed damping retention over millions of cycles without mass penalty, and they identified an optimal unfused powder threshold of approximately 3% for maximizing damping while maintaining mechanical reliability. Westbeld *et al* [15] examined process-induced variations such as local sintering and packing gradients in thin (less than 2 mm) flat cavities. Their results indicated that uneven powder compaction across cavity surfaces caused up to 30% variability in damping effectiveness, underscoring the need for precise control of powder retention and build orientation in LPBF processes.

2.2. Design and functional optimization

Several studies have addressed how geometric and design parameters govern damping efficiency. Ozcevik *et al* [16] conducted a 16-case parametric study on LPBF Inconel 718 specimens, showing that cavity volume fraction and placement significantly influenced the first and second vibration modes. Damping increased up to tenfold when cavities were positioned at displacement antinodes and occupied 3%–6% of the total volume. Oel *et al* [17] introduced mode-selective damping by tailoring cavity placement along the mode-shape displacement of steel beams. They achieved damping-ratio enhancements of up to 70 for the targeted mode, verifying a linear relationship between cavity displacement and damping improvement. Guo *et al* [18] demonstrated that subdividing a larger cavity (10 mm) into smaller 3–5 mm partitions effectively maintained damping performance at higher frequencies (200–2000 Hz). DEM simulations revealed that smaller cavities reduce clearance gaps, increase particle collision rates, and prevent powder sedimentation, key mechanisms enhancing high-frequency damping. Schmitz *et al* [19] confirmed that larger powder volumes within LPBF-fabricated cylinders increased energy dissipation through particle collision and friction, but observed diminishing returns when cavity diameters exceeded 8 mm due to powder settlement and localized stiffness loss. Tomita *et al* [20] extended the concept by integrating tuned PDs into locally resonant metamaterials fabricated via LPBF. Their hybrid design achieved vibration attenuation across wide frequency bands, exceeding 10 dB suppression in out-of-band regions, thus merging particle- and resonance-based damping mechanisms. Scott-Emuakpor *et al* [21] further emphasized the importance of reproducibility across different LPBF systems and powder batches. Their results underscored that optimized design tools and standardized build parameters are critical to maintaining consistent damping behavior under cyclic loading.

2.3. Analytical and computational models

To elucidate the governing mechanisms of particle damping and guide design optimization, a variety of analytical and computational models have been developed to capture both macroscopic vibration behavior and microscopic particle dynamics. Chawla [22] formulated an analytical model that explicitly relates the damping ratio to the geometry and excitation parameters of orthotropic cantilever beams containing perforated or cavity-filled regions. The model accounts for local stiffness reduction and mass distribution, providing closed-form predictions of modal damping as a function of cavity length-to-thickness ratio (typically 0.3–0.6) and excitation frequency up to 500 Hz. This framework enables rapid estimation of damping efficiency across multiple structural configurations and supports preliminary design screening without resorting to numerical simulation. Ye *et al.* [23] proposed an equivalent single-particle model for seismic applications to simplify computational analysis while maintaining physical fidelity. Their reduced-order formulation models the granular mass as a single lumped oscillator with effective stiffness and clearance parameters, capturing particle-wall impacts and frictional losses. Experimental validation on steel beam structures demonstrated that this approach can reproduce energy dissipation trends within 10% of full multi-particle simulations, making it highly suitable for large-scale structural analyses. Harduf *et al.* [24] developed a two-degree-of-freedom frictional system to describe nonlinear behavior in additively manufactured embedded PDs. In their model, the host structure and encapsulated powder bed are represented by coupled masses (m_1 and m_2) connected through a Coulomb-friction interface. Using Hilbert-transform-based system identification, they demonstrated that the structure exhibits a transition from linear to nonlinear response once the inertial force (m_2a) exceeds the friction limit (μN). Beyond this threshold, both the instantaneous damping ratio and natural frequency vary with amplitude: damping increases to a maximum near resonance and then decays as relative particle motion saturates. The model quantitatively replicated experimental trends of LPBF-fabricated beams containing embedded PD cavities. Liao *et al.* [25] coupled DEM and multi-body dynamics to capture nonlinear dissipation mechanisms in PDs. Their hybrid model resolved individual particle contacts to compute energy losses via normal restitution, tangential sliding, and rolling friction. They found that rolling friction accounted for 25%–40% of total energy dissipation under harmonic excitation, while collision-induced inelastic losses dominated at higher accelerations. The approach enables spatially resolved predictions of energy flow within cavities, bridging microscale particle interactions and macroscale damping behavior. Gagnon *et al.* [26] provided a comprehensive review of particle damping models, emphasizing the nonlinear, amplitude-dependent nature of granular damping. They highlighted that single-degree-of-freedom analytical models often neglect internal friction and particle-particle coupling, leading to underestimation of energy dissipation in multi-particle regimes. Their synthesis of numerical strategies recommends calibrated DEM simulations-validated against representative experiments, as the most reliable approach for capturing multi-axis effects, centrifugal loading, and state transitions between solid-like and gas-like particle behavior.

2.4. Research gaps and present study

Although particle damping via LPBF has been validated, key gaps remain. Specifically, the effects of powder packing density and post-printing volume compression are not well quantified, despite their clear influence on internal powder dynamics and damping behavior. Furthermore, process variabilities such as sintering and partial filling can suppress the intended damping effects, complicating their reliability for industrial deployment. To address these limitations, the present work investigates LPBF-integrated PDs subjected to controlled volume compression to systematically modify packing density. Using experimental shock and vibration testing and finite element analysis, we aim to distinguish the true effect of particle interactions from geometric contributions, thereby advancing the design of LPBF components with tunable damping. This paper extends our preliminary results on packing-density and compression effects [27, 28] and on modeling of LPBF PDs [29] by merging those threads into a unified framework, broadening the experiments (shock and shaker, multiple indentation levels with quantified uncertainty), and adding FEM that separates geometric stiffening from granular dissipation.

3. Experiment setup and methodology

This section details the experimental framework developed to investigate the influence of packing density and post-printing volume compression on the damping performance of LPBF-integrated PDs. It first describes the fabrication process of stainless steel cantilever beams containing internal powder-filled cavities designed to act as PDs. Subsequent subsections outline the controlled indentation procedure used to vary pocket volume and powder compaction, followed by descriptions of the shock and vibration testing

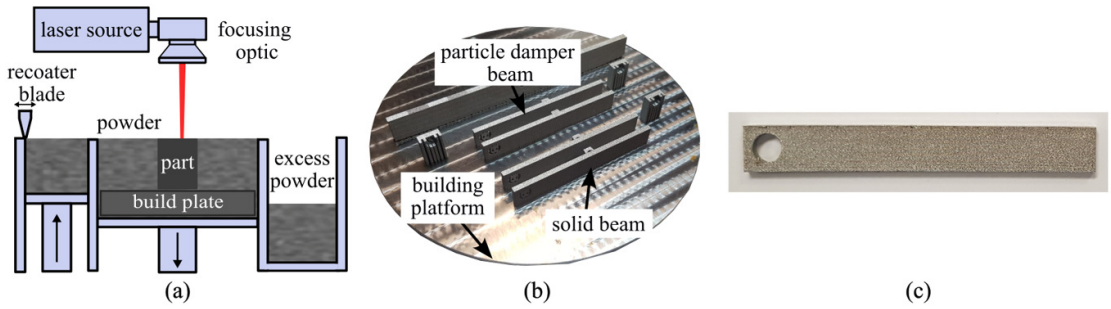

Figure 1. Particle damper test sample manufactured using LPBF with key components of the system annotated with (a) schematic of the LPBF process, (b) printing build plate showing the pre-cut samples, and (c) showing a fully processed particle damper beam.

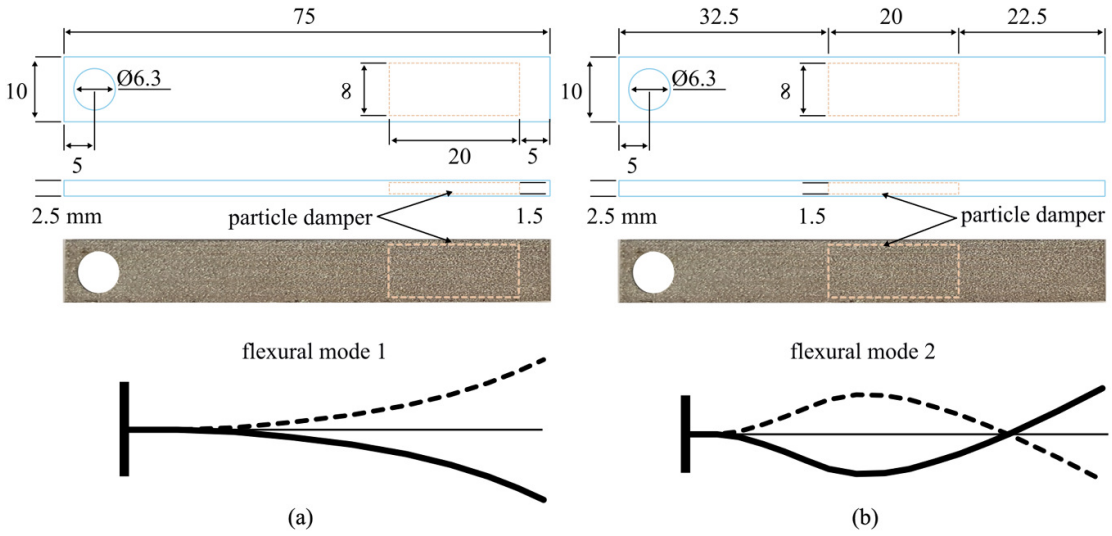

Figure 2. Particle damper test samples with key components and dimensions annotated, showing (a) sample targeting flexural mode one, and (b) sample targeting flexural mode 2 of a cantilever beam.

methods employed to quantify dynamic behavior under transient and harmonic excitations. Together, these methods establish a systematic approach to correlate manufacturing-induced modifications with vibration suppression characteristics, forming the basis for both the experimental and modeling analyses presented in later sections.

3.1. PD fabrication

In this research, cantilever beams were fabricated using 316 L stainless steel powder with an AconityMIDI LPBF printer, as shown in figure 1. The gas-atomized powder was supplied by Carpenter Technology Corporation, with a particle-size distribution of 15–45 μm and a mean of approximately 30 μm. Each beam measures 75 mm $\times$ 10 mm with a thickness of 2.5 mm. A 20 mm $\times$ 8 mm internal pocket with a thickness of 1.5 mm was included for the PD. Note that the thickness of the pocket is approximately 50 times of the mean particle size, expecting natural packing of the powders inside of the pocket without sintering. In the shock test configuration, the pocket is positioned 5 mm from the top (figure 2(a)), whereas in the vibration test configuration, the pocket is centered (figure 2(b)). This was done to target the first and second flexural modes of the cantilever beam respectively, allowing the study of the PD's influence on different mode shapes. The key printing parameters were: layer thickness of 30 μm, laser power of 200 W, scan speed of 800 mm s^{-1}, laser spot size of 100 μm, and hatch spacing of 100 μm. During printing, the build chamber was purged with argon to maintain the oxygen level below 100 ppm. A zig–zag hatch scanning strategy was employed, with the scan orientation rotating 67° between successive layers. A solid beam with the same dimensions and process parameters was also printed as a reference.

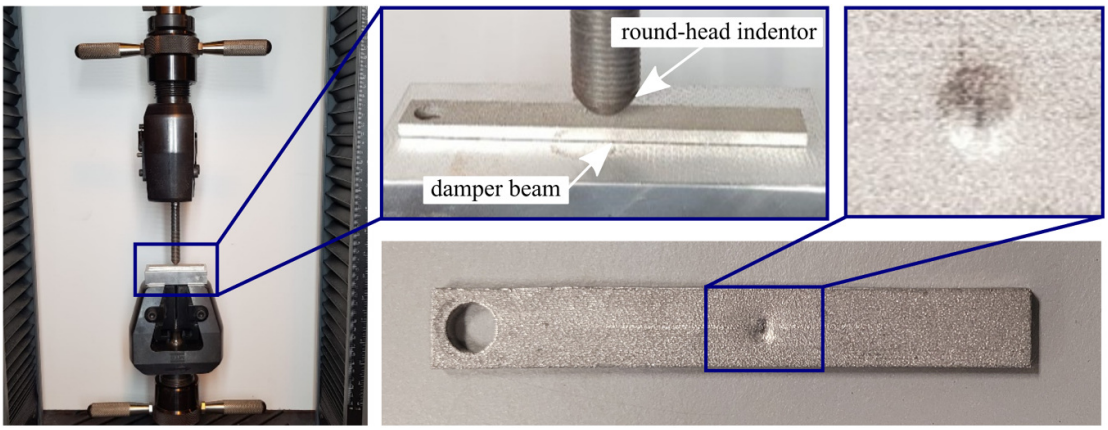

Figure 3. Indentation setup using an electromechanical load frame, with inset showing the resulting indent on the particle damper beam.

3.2. Volume compressing

The PD beams were subjected to varying levels of compression through an indentation process performed using an MTS Exceed E43 electromechanical load frame, as shown in figure 3. The first indentation was applied with a 2000 N force on the top surface of the particle pocket, followed by the additional indentations at the same location, each with a 1000 N force. This incremental loading approach was used to progressively increase the packing density of the powder within the pocket.

While the indentation process provides a controlled method to reduce the pocket volume and increase the effective packing density of the powder within the cavity, the internal distribution of particles after indentation cannot be directly observed in the present study. The compaction process may lead to local variations in particle packing density due to particle rearrangement and frictional interactions with the cavity walls. In this work, changes in packing density are inferred indirectly from the measured indentation depth and the corresponding pocket volume reduction obtained through surface topography measurements. Direct characterization of the internal particle distribution would require non-destructive imaging techniques such as x-ray computed tomography (XCT), which are considered for future work.

3.3. Shock test

Following the indentation process, surface topography measurements are recorded using a Keyence VHX-5000 digital microscope. The topographical images of the beam, both prior to and subsequent to the indentation, are illustrated in figure 4. The minimum and maximum surface heights derived from these measurements are detailed in table 1.

To induce shock in the electronic assembly, the sample is mounted onto a mass that is dropped onto a seismic base. The sudden deceleration causes an impulse excitation, which is captured using two IEPE accelerometers (Model 352A92 by PCB Piezotronics) that are fixed directly to the samples. Trials were conducted using the Lansmont P30 shock test system with a mount designed to secure two samples in a cantilever beam configuration, as shown in figure 5. The samples were mounted in pairs to study the response of the PD beam in reference to a solid beam with no pocket. This enabled a direct comparison of all four cases of damping with a single reference point. The experiment is conducted by dropping the samples from a height of approximately 75 mm to generate the free vibration response, which gets captured by the accelerometers at a sampling rate of 52 000 S s^{-1} using a sound and vibration module (NI 9234 from National Instruments). The signal obtained during free vibration response is then used to deduce the damping properties of the PD.

3.4. Vibration test

Two indentations are done on the PD beam with the same procedure as in the shock test. To accurately quantify the volume of the indentation, topography scans are taken before and after each indentation using a digital microscope. The topography imaging results are shown in figure 6 for all 3 cases, with the color bar indicating depth. To further investigate the dynamics of the PDs, a frequency response analysis is conducted using continuous excitation.

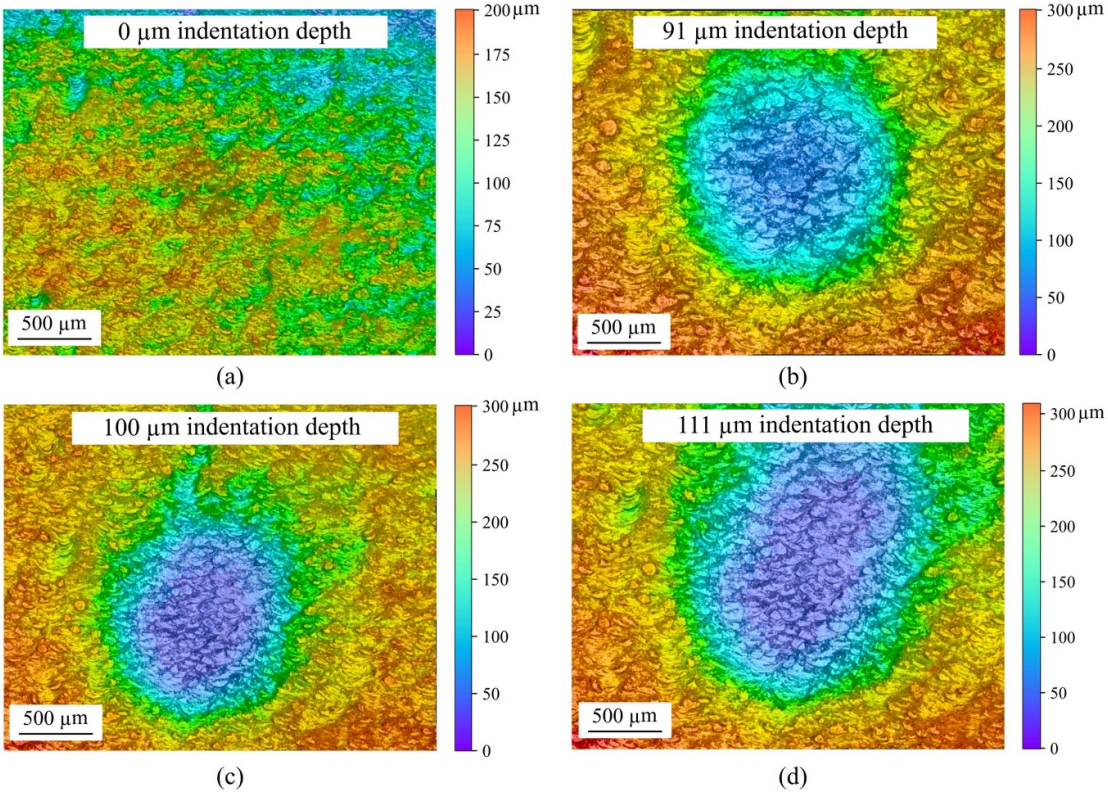

Figure 4. Microscope topography images of the particle damper beam surface: (a) prior to indentation (0 μm); (b) with a 91 μm indentation; (c) with a 99 μm indentation; and (d) with a 111 μm indentation.

Table 1. Surface height change of the particle damper beam.

particle damper beam	min-height (μm)	max-height (μm)
before indent	37.44	210.70
after first indent	0	301.77
after second indent	0	310.56
after third indent	3.93	322.08

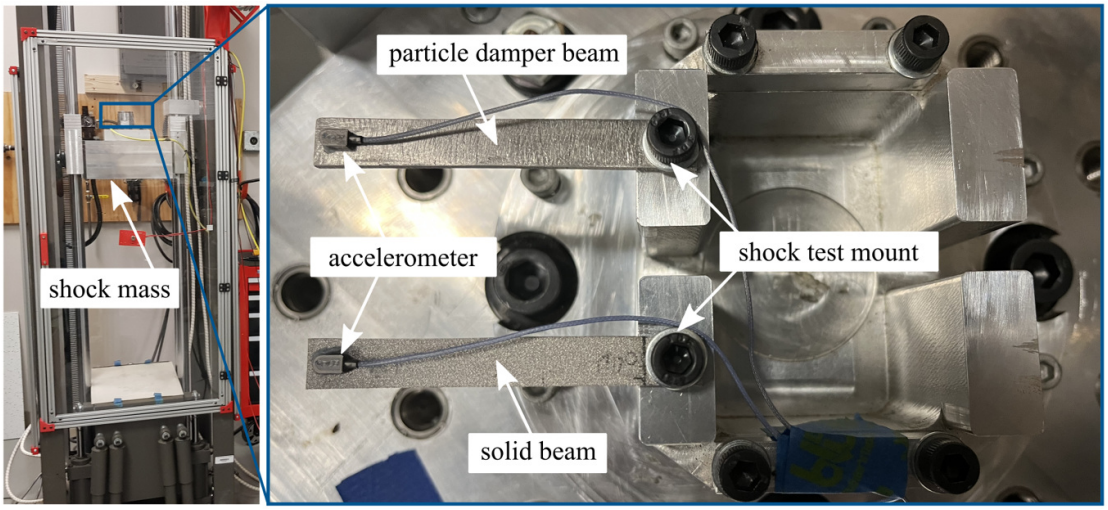

Figure 5. Experimental setup for the shock test excitation of the particle damper with key components annotated, showing the solid and particle damper beams.

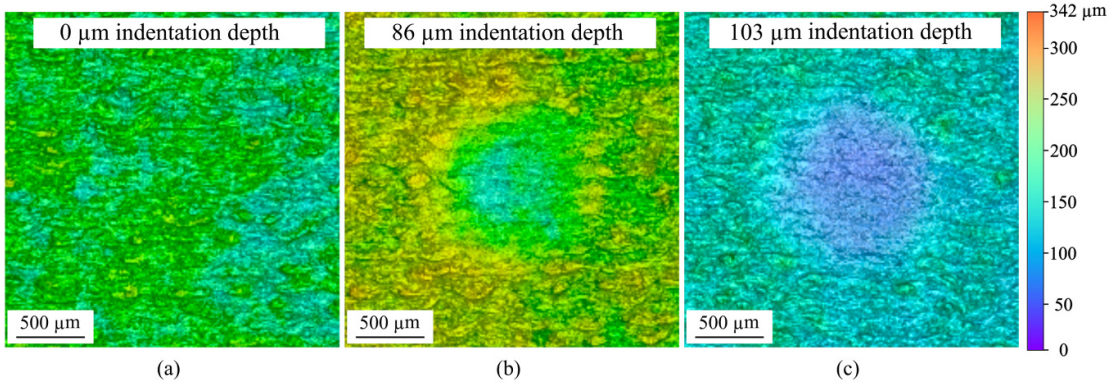

Figure 6. Microscope topography images of the particle damper beam surface: (a) prior to indentation (0 μm); (b) with an 86 μm indentation; and (c) with a 103 μm indentation.

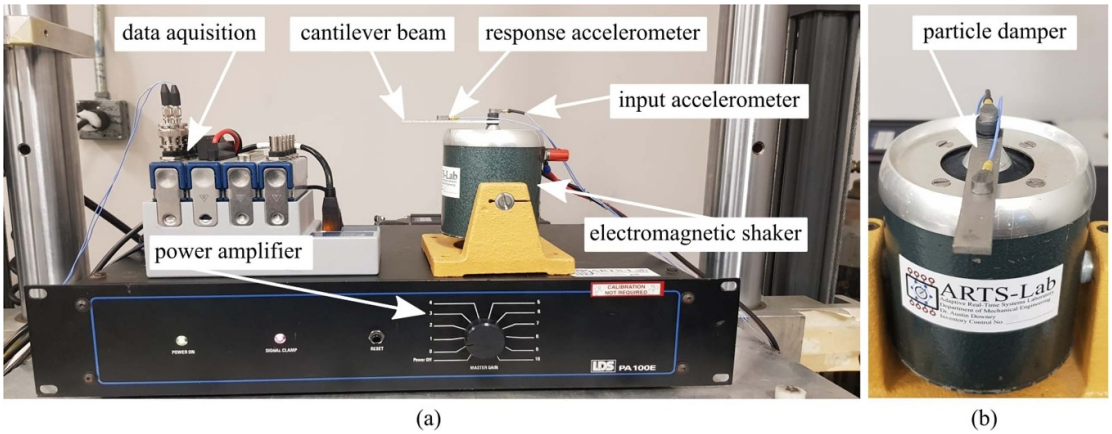

Figure 7. Frequency response experimental apparatus with (a) showing key components; (b) A close up of accelerometer placement on the particle damper beam.

As presented in figure 7, an experimental apparatus is designed to induce continuous excitation into the sample while measuring the response. This experiment aims to study the effects of the particle packing factor inside the damper pocket and its ability to suppress vibrations. An electromagnetic shaker is used to induce a frequency sweep excitation, while two accelerometers are used to capture both the input into the sample and its response to deduce an input-output relationship. This is later used to aid in developing a transfer function model representing the frequency response of the damper. For this test, the samples were manufactured with the PD pocket placed at the point of maximum deflection of the second flexural mode of a cantilever beam. This design decision was made due to that mode's relatively low dependency on the fixity, which aided in the repeatability of the experiment when samples are swapped.

4. Simulation validation

To investigate the influence of pocket geometry and internal powder behavior on structural dynamics, finite element models of the LPBF-fabricated cantilever beams were developed using FEA. Five beam configurations were simulated: (1) a solid beam without an internal pocket, (2) a beam with an empty cavity at the end representing the damper pocket as in figure 2(a); (3) a beam with a compliant filler region inside the end pocket; (4) a beam with an empty cavity in the center representing the damper pocket as in figure 2(b); and (5) a beam with a compliant filler region inside the center pocket. All beams were assigned the same mechanical properties determined by initially using the properties of 316 L stainless steel, then adjusting the elastic modulus such that the first mode of the solid beam in the simulation matched the first mode of the experimental solid beam. The beams were fixed at the through-hole to replicate the cantilever setup used in experiments. For beams with the compliant filler

Table 2. Finite element simulation material parameters for the solid and compliant filler regions.

Material property	Solid 316 L	Compliant filler 316 L
Elastic modulus (Pa)	1.80×10^{11}	9.65×10^{9}
Poisson ratio	0.29	0.25
Mass density (kg m^{-3})	7800	4880

region, separate material properties were used. The density of this region was determined by filling a similar pocket in a discrete element simulation with particles of similar size to the powder used to make the beams, and measuring the total mass of particles compared to the pocket. Elastic modulus and Poisson's ratio of the compliant filler region were estimated based on experimental results of packed 316 L powder gathered by Carnavas and Page [30]. All material property values can be found in table 2. The models were meshed using first-order hexahedral elements to capture complex geometry while maintaining reasonable computational cost. Modal and frequency response analyses were performed to identify changes in natural frequencies and deformation modes due to the presence of the pocket and its contents.

It should be noted that the present finite element model approximates the particle-filled cavity as a compliant continuum material with reduced elastic modulus. While this approach allows efficient evaluation of the global structural dynamics and the influence of pocket geometry, it does not explicitly capture the discrete particle interactions that govern energy dissipation in PDs. In particular, mechanisms such as particle-particle collisions, particle-wall impacts, frictional sliding, and amplitude-dependent rearrangement are inherently nonlinear and cannot be represented by a continuum approximation. More detailed modeling approaches, such as DEM simulations [31] or coupled FEM-DEM frameworks, could explicitly resolve these particle interactions and provide more accurate predictions of damping behavior. Such approaches represent a promising direction for future work.

5. Results

This section presents the experimental and numerical findings used to evaluate the damping behavior of LPBF-integrated PDs under varying packing densities and pocket compressions. The results are organized to first establish, through finite element simulations, that the observed vibration suppression originates from particle interactions rather than geometric changes to the structure. The following subsections then describe the shock test results, which quantify the effect of indentation-induced compaction on transient vibration decay, and the vibration test results, which provide frequency-domain insights through transfer function modeling. Together, these results validate the proposed methodology and demonstrate the tunability of damping performance in LPBF-fabricated components through controlled post-processing.

5.1. Simulation results

To validate that the observed damping behavior arises from internal particle interactions rather than geometric changes to the pocket or surrounding structure, finite element simulations were conducted using FEM. Two configurations for pockets positioned at the end and center of the beam were analyzed: one with a hollow pocket and another where the damper pocket was modeled as a compliant region mimicking the mechanical properties of a porous particle aggregate. Preliminary simulation results shown in table 3 indicated that the frequency response of the beam with porous-filled pockets closely matched, and in some cases, exceeded the modal frequencies observed experimentally, confirming a measurable shift in dynamic behavior attributable to particle interactions within the damper region.

Notably, mode shapes remained consistent across models, as seen in figure 8, suggesting that the primary damping source is not structural deformation but internal energy dissipation within the pocket. These simulations provide strong support for the conclusion that the damping effect is dominated by the PD and not by the change in material properties at the pocket region, reinforcing the experimental findings presented in the following section 5.3.

5.2. Shock test results

In figure 9, the free vibration response of the sample is presented, where (a) shows the original PD (0 μm) in comparison to the reference beam and (b) compares the 111 μm indentation to the same reference. The results indicate higher damping in case (a), proven by the rapid decay of the signal when

Table 3. Finite element simulation results for the solid, hollow, and porous-filled particle beams.

beam type	first mode frequency (Hz)	second mode frequency (Hz)
solid beam	428.70	2668.0
hollow end particle damper beam	504.86	2686.0
porous-filled end particle damper beam	452.73	2649.4
hollow center particle damper beam	438.69	2816.5
porous-filled center particle damper beam	427.76	2688.4

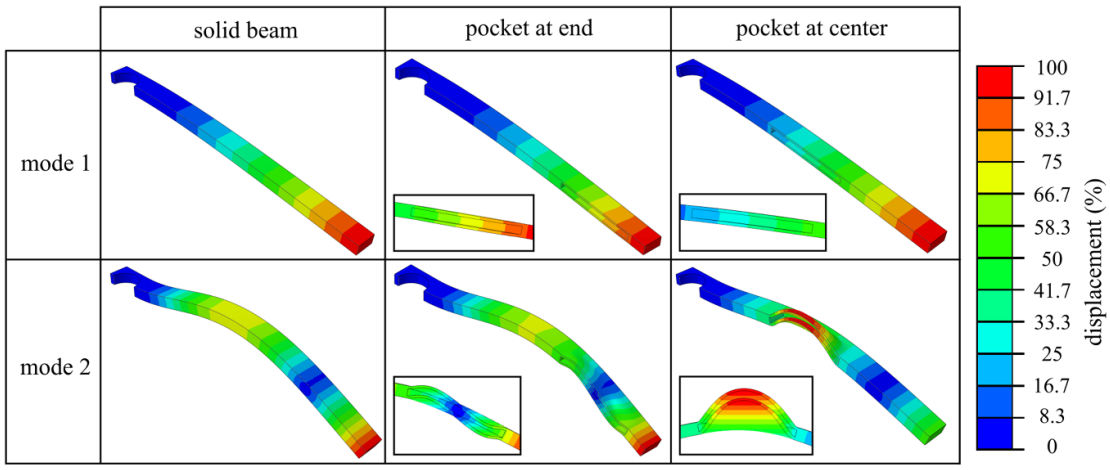

Figure 8. Finite element simulation for the solid beam and the pocket with porous-filled particles inside, with color indicating percent of maximum displacement.

examined against the response of the 111 μm indented beam. This was expected as the indentation increases the particles' packing factor, limiting the relative motion between particles. This behavior can be explained through the mechanics of granular damping. PDs dissipate vibrational energy primarily through inelastic particle-particle and particle-wall collisions, as well as frictional sliding between particles. When the particle packing density increases due to indentation, the available free volume within the cavity decreases, restricting the relative motion of the particles. As a result, the frequency and intensity of particle collisions are reduced, which lowers the amount of energy dissipated during each vibration cycle. In highly compacted states, the particle assembly behaves more like a constrained granular solid rather than a freely moving particle ensemble, reducing collision-based energy dissipation. Similar transitions between mobile and constrained particle behavior have been reported in prior studies of granular damping systems. This is further proven by examining all 4 cases of PDs in (c), where a clear pattern is shown with the decay profiles approaching that of the solid beam as the packing factor of the pockets is increased.

A system for comparing the performance across all damping cases was necessary due to the nonlinear nature of the PDs' impulse response. The Q factor was adopted as the metric, and a windowed peak detection algorithm was developed to calculate the decay profiles. The Q factor is a dimensionless parameter that quantifies the degree of underdamping in an oscillator or resonator [32]. A higher Q value indicates lower energy dissipation, allowing the system to sustain oscillations for a longer duration. The window length was chosen to exclude the system's initial transient response and the low signal-to-noise ratio at the end of the decay curve. This approach ensures a more accurate representation of the decay behavior necessary for Q factor calculation. The results, averaged over ten trials per case, are presented in table 4. The data show that the uncompressed PD exhibits the highest damping. As the particles are increasingly compacted due to indentation, the damping effect decreases. It is also observed that the damping behavior approaches that of the solid beam as the packing factor increases.

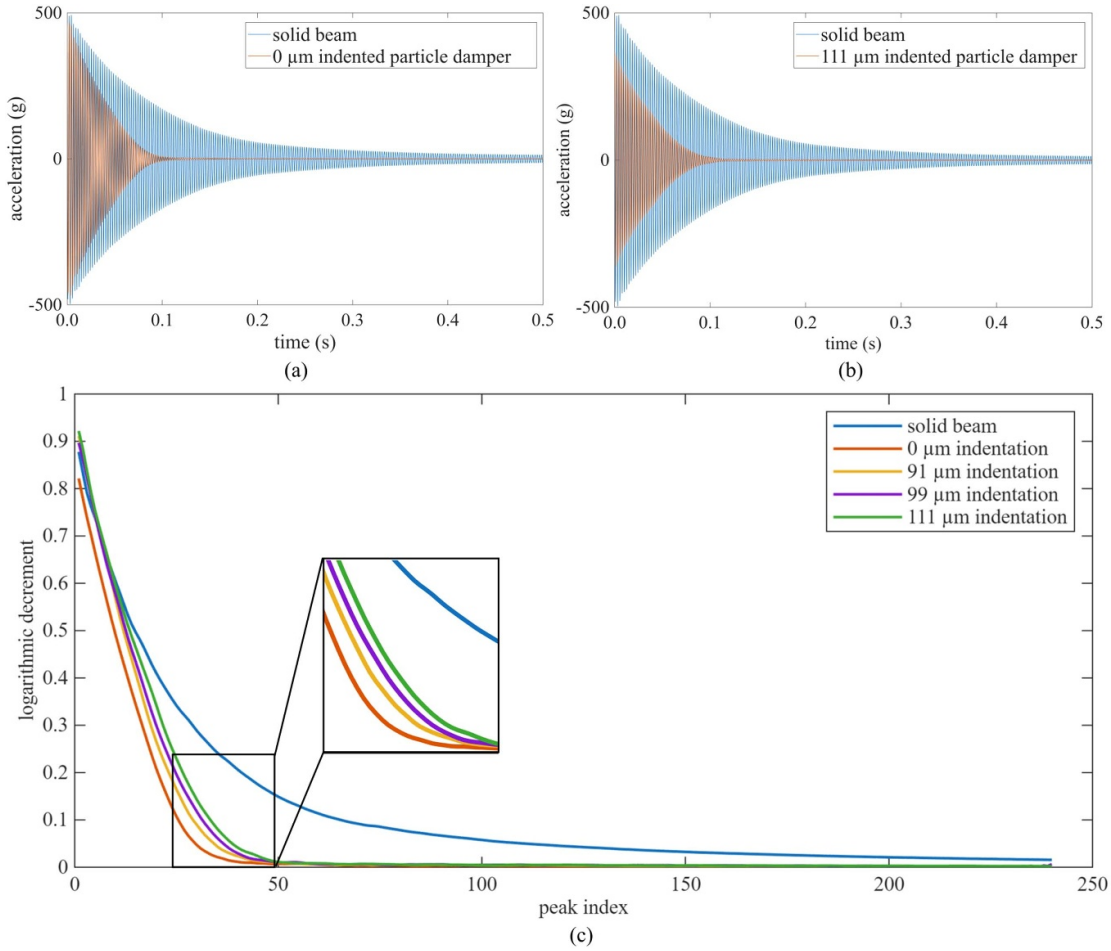

Figure 9. The vibration curves and decay rate: (a) the free vibration response of the solid beam and particle damper beam before indent (0 μm); (b) the free vibration response for the solid beam and particle damper beam with a 111 μm indentation; and (c) decay rates for the solid beam and particle damper beams.

Table 4. Shock test result for the solid and particle damper beam.

test sample	max frequency(Hz)	damping ratio	Q factor	Q factor standard deviation
solid beam	428.7	0.002 87	174.8	1.89
particle beam	416.0	0.004 30	116.7	4.88
91 μm indentation	425.7	0.004 20	119.4	4.52
99 μm indentation	425.8	0.004 08	122.8	4.48
111 μm indentation	428.7	0.004 01	124.6	4.17

When examining the decay profiles of the free vibration responses shown in figure 9(c), a rapid logarithmic decrement indicates highly nonlinear damping behavior [10]. The solid beam displays the slowest decay rate, whereas the decay curves for the PDs become increasingly steep as the indentation magnitude decreases. The unindented beam (0 μm) exhibits the highest damping characteristics, further supporting the role of the free-moving particles within the cavity in effectively suppressing shock through energy dissipation.

5.3. Vibration test results

In this section, the results from the vibration experiment are presented in figure 10 and discussed along with a transfer-function modeling approach used to characterize the global frequency response of the PD beam within the frequency range of the second flexural mode. The goal of this modeling approach is to represent the dynamic response of the beam-damper system as a whole, rather than to explicitly model the intricate particle-particle and particle-wall dynamics within the pocket. Using the data collected during the experimental phase, an S-domain transfer-function model was developed for the original, unindented particle-damper beam shown in figure 2(b). Multiple experimental trials were employed,

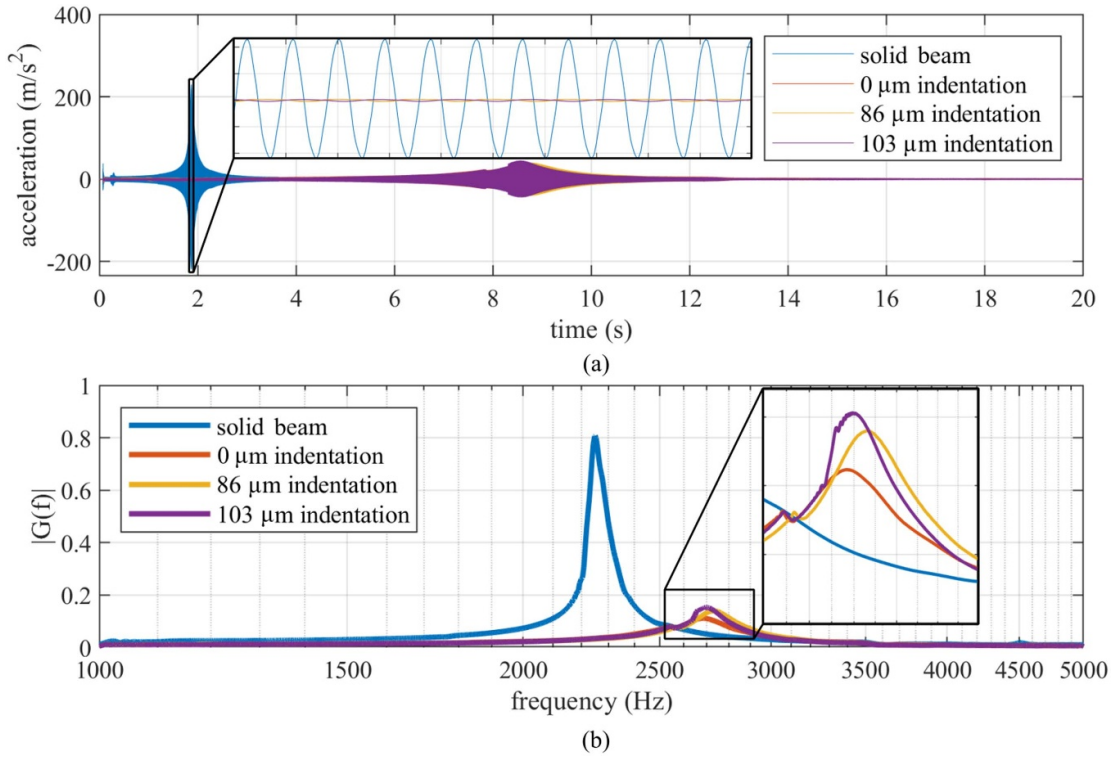

Figure 10. Frequency response experimental results showing (a) time-domain; and (b) frequency-domain responses of the solid beam and the particle damper under three packing-factor cases, with the peaks representing the resonant frequency of the second flexural mode.

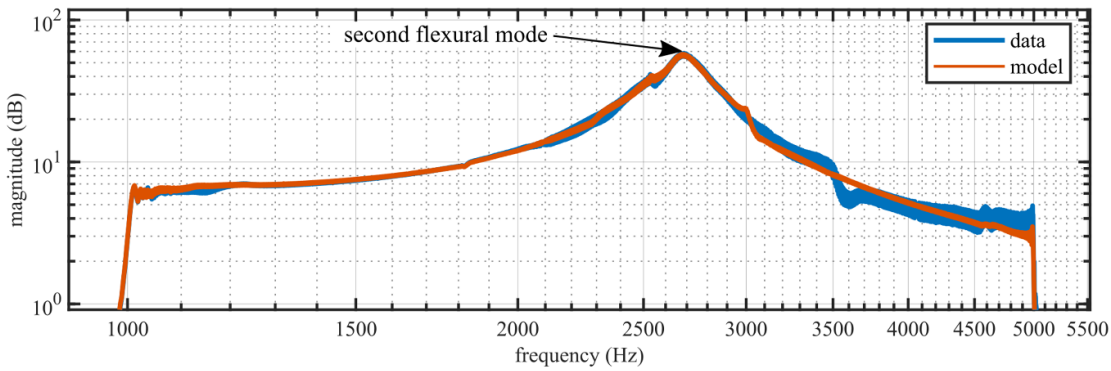

Figure 11. Magnitude plot of the frequency response of the unindented particle damper along with the transfer function model.

and the dataset was partitioned 50–50 into training and validation subsets. A grid search was performed to determine the optimal model order. To avoid overfitting and ensure generalizability, model performance was evaluated using data not included in the training process. The grid search identified a transfer function with six zeros and seven poles, achieving a fit of 91.25% and a mean squared error of 0.3746 $(\mathrm{m/s^2})^2$, as presented in equation (1). Model training was carried out using gradient descent with 100 iterations and a tolerance of 0.001. The corresponding frequency-domain response of the model, evaluated against the validation dataset, is illustrated in figure 11.

$$G(s) = \frac{-1.165\times10^{5}s^{6}+1.412\times10^{10}s^{5}+2.044\times10^{14}s^{4}+3.236\times10^{17}s^{3}+3.211\times10^{22}s^{2}-1.077\times10^{27}s-6.511\times10^{30}}{s^{7}+1.348\times10^{6}s^{6}-3.129\times10^{10}s^{5}+3.005\times10^{14}s^{4}-1.879\times10^{19}s^{3}-9.971\times10^{22}s^{2}-2.750\times10^{27}s-2.194\times10^{31}} \quad (1)$$

6. Conclusion and future work

This study investigated the damping behavior of LPBF-manufactured cantilever beams with embedded PDs by examining the effects of post-manufacturing pocket volume changes and powder packing density. Internal cavities filled with unfused powder were intentionally incorporated during fabrication, enabling integrated passive damping without additional assembly. To simulate changes in packing density, the pocket region was indented in three stages using controlled compressive loading. Damping performance was evaluated through both shock and shaker testing, with a solid beam used as a reference.

Experimental results confirmed that PDs significantly reduce vibration amplitude compared to solid beams. However, as the pocket volume decreased due to indentation, the powder became more densely packed, which diminished its ability to dissipate energy. This trend represents a key inverse relationship, as the increased packing factor caused by reduced pocket volume led to decreased damping performance. Despite this reduction, indented PD beams still exhibited faster vibration decay than solid beams, highlighting the inherent advantages of the embedded damper concept. Importantly, the fact that the Q factor was affected at all suggests that it may be possible to influence it in a positive direction. In particular, since indentation decreases pocket volume and increases packing factor, the inverse approach, expanding the pocket to increase available volume, could lower the packing factor and potentially improve energy dissipation in future designs, paving the way for future research on the tunability of embedded dampers.

To further clarify the source of damping, Abaqus finite element simulations were performed. These models helped distinguish whether observed vibration changes stemmed from particle behavior or geometric deformation of the beam. A transfer function model was also developed to characterize the dynamic response in the frequency domain, providing insights into both magnitude and phase behavior under continuous excitation.

Overall, LPBF-integrated PDs present a promising alternative to traditional damping systems, offering benefits such as reduced weight, material homogeneity, acoustic emission mitigation, and structural integration. This work validated the feasibility of tuning damping performance by altering internal pocket characteristics and demonstrated the capability to target specific modal resonances through geometric design. Future efforts will focus on quantifying powder density more precisely, extending evaluations to multiple mode shapes and loading scenarios, and further enhancing the predictive modeling of PD behavior. These advancements aim to support the development of multifunctional, self-damping components in next-generation structural systems.

While this study demonstrates the feasibility of tuning LPBF-integrated PDs through packing density and volume compression, several limitations remain. First, accurate quantification of powder packing density before and after indentation is still lacking; future efforts could utilize non-destructive techniques such as XCT or neutron imaging. Second, the current FEM simulations approximate the granular media as a compliant continuum, which may oversimplify the highly nonlinear behavior of particle interactions. Incorporating DEM or coupled FEM-DEM approaches would enable a more accurate representation of inter-particle collisions, friction, and dynamic rearrangement.

Acknowledgment

This material is based, in part, upon work supported by the South Carolina Space Grant Consortium, United States under Grant 21-117-RID RGP-SC-009 and 25-073-REAP-SC-001. This work is also partially supported by the National Institute of Standards & Technology, United States, under Grant Number 70NANB23H030; the National Science Foundation of the United States, through Grant CPS-2237696; the Air Force Office of Scientific Research (AFOSR), United States, through award no. FA9550-21-1-0083; and the National Science Foundation (NSF) through the NSF ASEE Fellowship. The support of these agencies is gratefully acknowledged. Any opinions, findings, conclusions, or recommendations expressed in this material are those of the authors and do not necessarily reflect the views of the South Carolina Space Grant Consortium, the National Institute of Standards & Technology, the National Science Foundation, the American Society for Engineering Education, or the United States Air Force.

Data availability statement

All data that support the findings of this study are included within the article (and any supplementary files).

Conflict of interests

The authors declare no conflict of interests

Author contributions

Joud N Satme 0000-0002-6769-8234
Data curation (equal), Formal analysis (equal), Investigation (equal), Writing – original draft (equal), Writing – review & editing (equal)

Yanzhou Fu 0000-0002-5471-9972
Investigation (equal), Methodology (equal), Validation (equal), Writing – original draft (equal), Writing – review & editing (equal)

Samuel Roberts 0009-0008-2175-0827
Data curation (equal), Formal analysis (equal)

Austin R J Downey 0000-0002-5524-2416
Conceptualization (equal), Funding acquisition (equal), Project administration (equal)

Tianyu Zhang 0000-0002-5046-7392
Conceptualization (equal), Resources (equal)

Lang Yuan 0000-0002-6894-5030
Conceptualization (equal), Resources (equal), Writing – review & editing (equal)

Daniel Kiracofe
Supervision (equal), Validation (equal), Writing – review & editing (equal)

References

[1] Alkhatib R and Golnaraghi M 2003 *Shock Vib. Dig.* **35** 367
[2] Randall R B 2021 *Vibration-Based Condition Monitoring: Industrial, Automotive and Aerospace Applications* (Wiley)
[3] Downey A and Micheli L 2024 Vibration Mechanics: a practical Introduction for Mechanical, Civil, and Aerospace Engineers Zenodo https://doi.org/10.5281/ZENODO.12539013
[4] Sánchez M and Manuel Carlevaro C 2013 *J. Sound Vib.* **332** 2070–80
[5] Fisco N R and Adeli H 2011 *Sci. Iran.* **18** 275–84
[6] Fu Y, Downey A R, Yuan L, Zhang T, Pratt A and Balogun Y 2022 *J. Manuf. Process.* **75** 693–710
[7] Chowdhury S, Yadaiah N, Prakash C, Ramakrishna S, Dixit S, Gupta L R and Buddhi D 2022 *J. Mater. Res. Technol.* **20** 2109–72
[8] Ehlers T, Oel M, Tatzko S, Kleyman G, Niedermeyer J, Wallaschek J and Lachmayer R 2023 *Procedia CIRP* **119** 891–6
[9] Westbeld J, von Coburg F and Höfer P 2023 *Prog. Addit. Manuf.* **8** 745–57
[10] Ehlers T, Tatzko S, Wallaschek J and Lachmayer R 2021 *Addit. Manuf.* **38** 101752
[11] Guo H, Ichikawa K, Sakai H, Zhang H, Zhang X, Tsuruta K, Makihara K and Takezawa A 2022 *Powder Technol.* **396** 696–709
[12] Schmitz T, Gomez M, Ray B, Heikkenen E, Sisco K, Haines M and Osborne J S 2020 *Precis. Eng.* **66** 110–24
[13] Scott-Emuakpor O E, George T, Beck J, Runyon B D, O'Hara R, Holycross C and Sheridan L 2019 Inherent damping sustainability study on additively manufactured nickel-based alloys for critical part *AIAA Scitech 2019 Forum* p 0410
[14] Scott-Emuakpor O, George T, Runyon B, Holycross C, Langley B, Sheridan L, O'Hara R, Johnson P and Beck J 2018 Investigating damping performance of laser powder bed fused components with unique internal structures *Turbo Expo: Power for Land, Sea and Air* vol 51159 (American Society of Mechanical Engineers) p V07CT35A020
[15] Westbeld J, Dauenhauer D and Höfer P 2025 *Int. J. Adv. Manuf. Technol.* **139** 1815–29
[16] Ozcevik B, Soylemez E, Bediz B and Simsek U 2024 *Int. J. Adv. Manuf. Technol.* **130** 3917–28
[17] Oel M, Kleyman G, Jonkeren M, Tatzko S and Ehlers T 2025 *Prog. Addit. Manuf.* **10** 3739–50
[18] Guo H, Yoneoka R and Takezawa A 2024 *Powder Technol.* **439** 119675
[19] Schmitz T, Betters E and West J 2020 *Manuf. Lett.* **25** 1–5
[20] Tomita S, Masutani T and Sato H 2025 *J. Sound Vib.* **596** 118715
[21] Scott-Emuakpor O, Beck J, Runyon B and George T 2021 *Addit. Manuf.* **38** 101739
[22] Chawla K 2022 *Appl. Math. Modelling* **101** 716–28
[23] Ye H, Wang Y, Liu B and Jiang X 2019 *Appl. Sci.* **9** 2912
[24] Harduf Y, Setter E, Feldman M and Bucher I 2023 *Mech. Syst. Signal Process.* **187** 109928
[25] Liao C C, Chung Y C and Weng C 2023 *Nonlinear Dyn.* **111** 1–26
[26] Gagnon L, Morandini M and Ghiringhelli G L 2019 *J. Sound Vib.* **459** 114865
[27] Satme J N, Fu Y, Downey A R, Yuan L and Kiracofe D 2024 Impact of particle packing density on the frequency response of an additively manufactured particle damper *AIAA SCITECH 2024 Forum* (American Institute of Aeronautics and Astronautics)
[28] Fu Y, Joud S, Downey A R J, Yuan L, Zhang T and Kiracofe D 2025 Investigating Compressing Particle Damper Pockets in Beams Manufactured by Laser Powder Bed Fusion Additive Manufacturing *Special Topics in Structural Dynamics & Experimental Techniques* vol 5 (River Publishers) pp 139–44

[29] Roberts S, Fu Y, Satme J, Kiracofe D, Downey A R J and Yuan L 2025 Modeling post-process indenting using the discrete element method for particle density control in additively manufactured dampers *Active and Passive Smart Structures and Integrated Systems XIX*, ed S Tol, M A Nouh, J Yang, G Huang, X Li, Y Chen and C Sugino (SPIE)) p 60
[30] Carnavas P and Page N 1998 *J. Mater. Sci.* **33** 4647–55
[31] Roberts S, Fu Y, Satme J N, Kiracofe D, Downey A R and Yuan L 2025 Modeling post-process indenting using the discrete element method for particle density control in additively manufactured dampers *Active and Passive Smart Structures and Integrated Systems XIX* vol 13432 (SPIE)) pp 255–61
[32] Adhikari S 2017 *J. Appl. Phys.* **122** 144304